Taylor & Francis
Taylor & Francis Group

High Pressure Research
An International Journal

ISSN: 0895-7959 (Print) 1477-2299 (Online) Journal homepage: www.tandfonline.com/journals/ghpr20

Structural, elastic and thermodynamic properties of tetragonal and orthorhombic polymorphs of Sr_2GeN_2: an *ab initio* investigation

A. Bedjaoui, A. Bouhemadou & S. Bin-Omran

To cite this article: A. Bedjaoui, A. Bouhemadou & S. Bin-Omran (2016) Structural, elastic and thermodynamic properties of tetragonal and orthorhombic polymorphs of Sr_2GeN_2: an *ab initio* investigation, High Pressure Research, 36:2, 198-219, DOI: 10.1080/08957959.2016.1167202

To link to this article: https://doi.org/10.1080/08957959.2016.1167202

HIGH PRESSURE RESEARCH, 2016
VOL. 36, NO. 2, 198–219
http://dx.doi.org/10.1080/08957959.2016.1167202

Taylor & Francis
Taylor & Francis Group

Structural, elastic and thermodynamic properties of tetragonal and orthorhombic polymorphs of Sr_2GeN_2: an *ab initio* investigation

A. Bedjaoui[a], A. Bouhemadou[a] and S. Bin-Omran[b]

[a]Laboratory for Developing New Materials and Their Characterization, University of Setif 1, Setif, Algeria; [b]Department of Physics and Astronomy, College of Science, King Saud University, Riyadh, Saudi Arabia

ABSTRACT

The structural, elastic and thermodynamic properties of the α (tetragonal) and β (orthorhombic) polymorphs of the Sr_2GeN_2 compound have been examined in detail using *ab initio* density functional theory pseudopotential plane-wave calculations. Apart the structural properties at the ambient conditions, all present reported results are predicted for the first time. The calculated equilibrium lattice parameters and inter-atomic bond-lengths of the considered polymorphs are in good agreement with the available experimental data. It is found that α-Sr_2GeN_2 is energetically more stable than β-Sr_2GeN_2. The two examined polymorphs are very similar in their crystal structures and have almost identical local environments. The single-crystal and polycrystalline elastic parameters and related properties – including elastic constants, bulk, shear and Young's moduli, Poisson's ratio, anisotropy indexes, Pugh's criterion, elastic wave velocities and Debye temperature – have been predicted. Temperature and pressure dependence of some macroscopic properties – including the unit-cell volume, bulk modulus, volume thermal expansion coefficient, heat capacity and Debye temperature – have been evaluated using *ab initio* calculations combined with the quasi-harmonic Debye model.

ARTICLE HISTORY
Received 1 December 2015
Accepted 14 March 2016

KEYWORDS
Sr_2GeN_2 polymorphs; *ab initio* calculations; structural parameters; elastic constants; thermodynamic properties

1. Introduction

Because of their set of excellent useful properties (such as low compressibility, good thermal stability, chemical and radiation inertness and semiconducting), which allow important new technological applications (such as high-performance light-emitting devices, ultraviolet photodetectors, light-emitting diodes, lasers,[1,2] converting solar light into electricity, photocatalysis, hydrogen production,[3] lithium-ion batteries,[4] magnetic and electronic devices,[5,6] automotive engine wear parts, cutting tools and so on), nitride materials have gained increasing interest since the mid-1980s.

In the quest of other nitride materials having the interesting properties of the binary nitrides and at the same time having other new properties that allow other new

CONTACT A. Bouhemadou a_bouhemadou@yahoo.fr Laboratory for Developing New Materials and Their Characterization, University of Setif 1, 19000 Setif, Algeria.

applications that are limited by the properties of the binary nitrides, such as an optimal band gap for higher effectiveness of possible devices, high-performance chemical and radiation inertness, the attention has been drawn to ternary and quaternary nitrides.[7–25] Consequently, the number of synthesized ternary and quaternary nitrides has progressed rapidly over the last two decades. These new multinary nitrides provide a wider range of interesting mechanical, electrical, electronic, optical and chemical properties that make them potential candidates for probable new technological applications.

Some of the recently synthesized ternary nitrides are based on the germanium nitrides (GeN), such as the orthorhombic and tetragonal polymorphs of the strontium germanium nitrides, labeled as α-Sr_2GeN_2 and β-Sr_2GeN_2 polymorphs, respectively.[24,25] The α-Sr_2GeN_2 and β-Sr_2GeN_2 phases were synthesized as single-crystals by DiSalvo et al. [24,25] from the constituent elements in sealed Nb tubes at about 750°C, using liquid *Na* as a growth medium. These two Sr_2GeN_2 polymorphs have several quite similar properties, such as the unit-cell volume and bond-lengths. A differentiating factor of the crystalline structures of these two polymorphs is the relative orientation of theGeN_2 units in the lattice.[24,25] Figure 1 displays the unit-cells of the tetragonal and orthorhombic polymorphs of Sr_2GeN_2. As one can observe, the GeN_2 units belong to the plane [001] in the α-Sr_2GeN_2 crystal, while in the β-Sr_2GeN_2 crystal, they belong to the plane [100]. From Figure 1, one can observe that both α-Sr_2GeN_2 and β-Sr_2GeN_2 crystals are layered materials; the layers are stacked along the *c*-axis in α-Sr_2GeN_2, while in β-Sr_2GeN_2, they are stacked along the *a*-axis. The structural difference between these two compounds is due to the manner that adjacent planes are stacked. The stacking is carried out in an alternating manner for both compounds. In α-Sr_2GeN_2, the adjacent planes A and A′, which are stacked along the *c*-axis according to the following sequence: … AA′AA′AA′ … , are related by a 90° rotation, that is, A′ plane is produced by rotating the A plane by an angle of 90°. Whereas, in β-Sr_2GeN_2, the adjacent planes A and A′, which are stacked along the *a*-axis according to the following sequence: … AA′AA′AA′ … , are related by a translation of $(1/2)\vec{b}$, that is, A′ plane is a result of the translation of the A plane by $(1/2)\vec{b}$.

Apart the synthesis optimal conditions and structure features,[24,25] experimental data on α-Sr_2GeN_2 and β-Sr_2GeN_2 crystals are not available in the scientific literature. Theoretical investigations of these systems are also scarce; as far as we know, there is only one theoretical work,[26] which explored the electronic and optical properties of these compounds using full potential linearized augmented plane-wave calculations in the framework of the density functional theory. The reported theoretical results [26] reveal that α-Sr_2GeN_2 and β-Sr_2GeN_2 are very narrow band gap semiconductors. The ternary nitrides $\beta - Sr_2GeN_2$and $\beta - Sr_2GeN_2$ can be used as substrates for GeN-based devices. Other

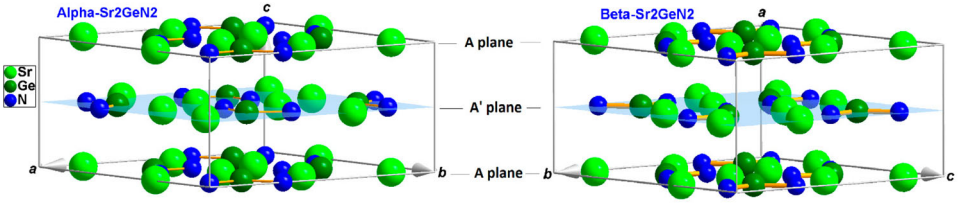

Figure 1. (Colour online) Unit-cell structures of the tetragonal and orthorhombic polymorphs of the Sr_2GeN_2 crystal (α-Sr_2GeN_2 and β-Sr_2GeN_2 phases, respectively).

eventual applications of these considered nitrides can be revealed from exploring and understanding their physical properties.

For optoelectronic device applications, semiconductor layers are commonly grown as thin epitaxial layers and superlattices on substrates. The lattice mismatch and difference in thermal expansion coefficients between epitaxial layers and substrates can cause large stresses in the epitaxial layers, which could affect their physical properties.[27–29] Hence, it is interesting and necessary for practical use to know: (i) the elastic constants, which describe the response of the material to the externally applied strains, and (ii) the evolution of the physical properties of these materials with pressure and temperature. The electronic and optical properties of the title nitrides have already been investigated by Zeyad and Reshak,[26] whereas, to the best of authors' knowledge, no theoretical or experimental studies of the elastic and thermodynamic properties for these two nitrides are available in the scientific literature. On other hand, it is worth noting that the former reported theoretical calculations [26] investigated α-Sr_2GeN_2 and β-Sr_2GeN_2 phases at zero temperature only without any thermal effects included. Commonly, measurements of the elastic constants and effects of pressure and temperature on physical proprieties of materials are very difficult. Therefore, the lack of experimental data on these properties can be fulfilled via theoretical simulation based on accurate *ab initio* calculations. Thus, the first main objective of the present work is accurate calculations of the elastic constants and related properties at ambient as well as elevated pressures up to 15GPa using *ab initio* pseudopotential plane-wave method (PP-PW) based on density functional theory. The second main objective is the exploration of the pressure and temperature effects on the unit-cell volume, bulk modulus, volume thermal expansion, isochoric heat capacity and Debye temperature of the title compounds using the PP-PW method in combination with the quasi-harmonic Debye model. We hope that the reported data can provide theoretical support to the existing experimental and theoretical data and provide a basis for future experimental and theoretical studies in order to have insight about eventual technological applications of the considered ternary nitrides α-Sr_2GeN_2 and β-Sr_2GeN_2. The paper is organized as follows. In Section 2, we give details of the computational method used in the present work. The obtained results and their discussion are presented in Section 3. A summary of the main results is provided in Section 4.

2. Computational details

All performed *ab initio* calculations in the present work were carried out using pseudopotential plane-wave (PP-PW) method in the framework of density functional theory as implemented in the CASTEP module.[30] The exchange-correlation effects were treated using the recent developed generalized gradient approximation of Perdew et al. [31], the so-called GGA-PBEsol, which is known to yield better results for solids. To take into account the contribution of core electrons, Vanderbilt ultra-soft pseudopotential [32] was employed. The Sr: $4s^2 4p^6 5s^2$, Ge: $4s^2 4p^2$ and N: $2s^2 2p^3$ orbitals were treated as electronic valence states. The Monkhorst–Pack scheme [33] was used for the *k*-points sampling in the Brillouin zone. A kinetic energy cutoff of 280 eV and *k*-mesh corresponding to a separation of 0.03 $Å^{-1}$ (0.04 $Å^{-1}$) in the reciprocal space for the α-Sr_2GeN_2 (β-Sr_2GeN_2) phase were used. These calculation parameters were chosen after careful convergence tests.

The optimized structural parameters were obtained using the Broyden–Fletcher–Goldfarb–Shanno minimization algorithm.[34] The lattice parameters and internal coordinates were relaxed until: (i) total energy variation was smaller than 5.0×10^{-6} eV/atom, (ii) the absolute value of force on any atom was less than 0.01 eV/Å, (iii) stress was smaller than 0.02 GPa and (iv) atomic displacement was smaller than 5.0×10^{-4} Å.

The elastic properties of single-crystal and polycrystalline aggregates of α-Sr_2GeN_2 and β-Sr_2GeN_2 compounds were explored by calculating their independent elastic constants C_{ij}, bulk modulus B, shear modulus G, Young's modulus E, Poisson's coefficient σ and related properties. The C_{ij} were obtained via linear fittings of the stress–strain curves computed from accurate *ab initio* calculations.[30] The main advantage of this method is the great reduction of the independent strain modes number compared to the *ab initio* total energy versus strain approach. The elastic stiffness tensor is related to the stress tensor and the strain tensor by Hooke's law. Since the stress tensor and the strain tensor are symmetric, the most general elastic stiffness tensor has only 21 non-zero independent components. For a tetragonal crystal, they are reduced to six independent components, namely C_{11}, C_{33}, C_{44}, C_{66}, C_{12} and C_{13}, and for an orthorhombic crystal, they are reduced to nine independent components, namely C_{11}, C_{22}, C_{33}, C_{44}, C_{55}, C_{66}, C_{12}, C_{13} and C_{23}. To determine the six independent elastic constants C_{ij} of the tetragonal system, two strain patterns – one with non-zero ε_{11} and ε_{23} components and the second with non-zero ε_{33} and ε_{12} components – were used. To obtain the nine independent components of the elastic tensor for the orthorhombic phase, three strain patterns – one with non-zero $\varepsilon_{23}$and ε_{23}components, second with non-zero ε_{22} and ε_{31} components and the third with non-zero ε_{33} and ε_{12} components – were used. The elastic constants were performed with the following convergence criteria: 1.0×10^{-6} eV/atom for the total energy, 0.002 eV/Å for the Hellman–Feynman force and 1.0×10^{-4} Å for the maximal ionic displacement. After calculating the single-crystal elastic constants C_{ij}, the polycrystalline elastic moduli and related properties were evaluated using the well-known Voigt–Reuss–Hill approximations.[35–37]

Knowledge of the behaviors of solids when they are under severe constraints such as high-pressure and high-temperature environment are of a great interest and importance for both the fundamental research and technological applications. To address this interest in the present work, pressure and temperature dependences of the unit-cell volume, bulk modulus, volume expansion coefficient, isochoric heat capacity and Debye temperature of both considered phases were explored using the PP-PW method [30] combined with the quasi-harmonic Debye model as implemented in Gibbs program.[38] Theoretical details about the quasi-harmonic Debye model are available in Blanco et al. [38].

3. Results and discussions

3.1. Structural properties

Knowledge of the equilibrium structural parameters of materials is necessary before investigating their physical and chemical properties using *ab initio* calculations. Information on the structural parameters of the investigated α and β polymorphs of Sr_2GeN_2, which were used as input data in the present calculations, were taken from [24,25]. The α-Sr_2GeN_2 compound crystallizes in a tetragonal structure, space group $P4_2/mbc$ (No. 135), with

eight unit formulas (*i.e.* 8 Sr_2GeN_2) per unit-cell ($Z = 8$), while the β-Sr_2GeN_2 polymorph crystallizes in an orthorhombic structure, space group *Cmac* (No. 64), with eight unit formulas per unit-cell ($Z = 8$) also.[24,25] This implies that the unit-cell of both polymorphs contains 40 atoms: 16 Sr, 16 N and 8 Ge. The atomic positions in the α-Sr_2GeN_2 crystal are Sr1 (x_{Sr1}, y_{Sr1}, 0), Sr2 (x_{Sr2}, y_{Sr2}, 0), Ge (x_{Ge}, y_{Ge}, 0), N1 (x_{N1}, y_{N1}, 0) and N2 (x_{N2}, y_{N2}, 0) and in the β-Sr_2GeN_2 crystal, they are Sr1 (0, y_{Sr1}, z_{Sr1}), Sr2 (0, y_{Sr2}, z_{Sr2}), Ge (0, y_{Ge}, z_{Sr2}), N1 (0, y_{N1}, z_{N1}) and N2 (*0*, y_{N2}, z_{N2}). The atoms are indexed in order to distinguish between the inequivalent crystallographic positions of the same chemical element. The equilibrium structural parameters at zero pressure and zero temperature for α-Sr_2GeN_2 and β-Sr_2GeN_2, calculated with full structural optimization including atomic positions, are listed in Tables 1 and 2 along with the available experimental values. The obtained equilibrium lattice parameters appear to be in very good agreement with their corresponding experimental data. For α-Sr_2GeN_2, the computed equilibrium lattice parameters a_0 and c_0 are slightly lower than the experimental values and the discrepancies are about −0.25% and −1.59%, respectively. For β-Sr_2GeN_2, the computed equilibrium lattice parameters a_0 and c_0 are slightly lower than the experimental values with relative deviations of about −1.54% and −0.92%, respectively, while the equilibrium lattice parameter b_0 is slightly higher than the experimental value with a relative deviation of about +0.18%.

Table 1. Calculated lattice parameters (a_0, b_0 and c_0, in Å), unit-cell volume (V_0, in Å^3), bulk modulus (B_0, in GPa) and its pressure derivative B', cohesive energy (E_{coh}, in eV/atom), formation enthalpy (ΔH, in eV/atom), inter-atomic distances (in Å) and bond-angle (in degree) for the tetragonal and orthorhombic polymorphs of Sr_2GeN_2 together with available experimental data for the sake of comparison.

	α-Sr_2GeN_2		β-Sr_2GeN_2	
Property	Present	Expt. [24]	Present	Expt. [25]
a_0	11.7434	11.773	5.3565	5.441
b_0	11.7434	11.773	11.3982	11.377
c_0	5.3233	5.409	12.1166	12.229
V_0	734.126	749.7	739.776	756.9
B_0	68.569[a], 69.426[b], 69.00[c], 68.808[d] 70.77[e], 70.23[f]		66.614[a], 67.521[b], 67.82[c], 66.092[d] 68.21[e], 67.71[f]	
B'	4.533[a], 4.161[b], 3.40[c], 4.866[d]		4.633[a], 4.238[b], 3.35[c], 5.048[d]	
E_{coh}	−5.907		−5.898	
ΔH	−1.500		−1.491	
Ge–N1	1.882	1.851	1.904	1.879
Ge–N2	1.898	1.877	1.875	1.852
Sr1–N1	2.547	2.562	2.653	2.662
Sr1–N1*	2.670	2.713	2.700	2.744
Sr1–N1	2.779	2.807	–	–
Sr1–N2	2.603	2.628	2.554	2.584
Sr1–N2	–	–	2.756	2.787
Sr2–N1	2.664	2.681	2.530	2.561
Sr2–N1	–	–	2.723	2.737
Sr2–N2	2.535	2.564	2.656	2.653
Sr2–N2*	2.695	2.741	2.684	2.728
Sr2–N2	2.740	2.742	–	–
N1–Ge–N2	113.23	113.51	113.49	113.17

[a]Calculated from Birch–Murnaghan *P*–*V* EOS.[39]
[b]Calculated from Murnaghan *P*–*V* EOS.[40]
[c]Calculated from Birch–Murnaghan *E*–*V* EOS.[41]
[d]Calculated from Vinet *E*–*V* EOS.[42]
[e]Calculated from third-order polynomial *V*–*P* fitting.
[f]Calculated from linear compressibilities.
*The bonds that ensure the coherence between adjacent planes.

Table 2. Calculated atomic positions for the α-Sr_2GeN_2 and β-Sr_2GeN_2 crystals along with available theoretical and experimental findings for comparison.

	Present work			Experiments			Other calculations [26]		
atom	*x/a*	*y/b*	*z/c*	*x/b*	*y/c*	*z/c*	*x/b*	*y/c*	*z/c*
α-Sr_2GeN_2					[24]				
Sr(1)	0.36669	0.42058	0	0.3671	0.4190	0	0.36642	0.42015	0
Sr(2)	0.02219	0.34864	0	0.0224	0.3482	0	0.02167	0.34869	0
Ge	0.25614	0.15184	0	0.2559	0.1514	0	0.25572	0.15083	0
N(1)	0.09687	0.13442	0	0.0996	0.1340	0	0.09734	0.13392	0
N(2)	0.33567	0.01112	0	0.3353	0.0131	0	0.33538	0.01088	0
β-Sr_2GeN_2					[25]				
Sr(1)	0	0.04757	0.35851	0	0.0479	0.35760	0	0.04768	0.35739
Sr(2)	0	0.35563	0.44232	0	0.3564	0.44110	0	0.35556	0.44286
Ge	0	0.23881	0.18162	0	0.2398	0.17990	0	0.24001	0.18031
N(1)	0	0.07730	0.14139	0	0.0797	0.14190	0	0.07835	0.14125
N(2)	0	0.34079	0.06024	0	0.3389	0.05970	0	0.34058	0.05971

The calculated equilibrium unit-cell volume is slightly lower than the measured one by about −2.08% in α-Sr_2GeN_2 and about −2.26% in β-Sr_2GeN_2. This observed slight relative deviation of the calculated results from the measured ones could be attributed to the fact that our values are calculated at zero temperature while the corresponding experimental ones are measured at ambient temperature; the volume increases with the increasing temperature. This good consistency between our calculated equilibrium lattice parameters and the corresponding measured ones constitutes a proof of reliability of the present calculations and accuracy of the reported results. We note that the two considered polymorphs have practically the same unit-cell volume; the unit-cell volume of β-Sr_2GeN_2 is slightly larger than that of α-Sr_2GeN_2 by about 0.76%. The optimized atomic positions and inter-atomic bond-lengths of α-Sr_2GeN_2 and β-Sr_2GeN_2 are also in good agreement with the corresponding experimental data. From Table 1 data, one can observe that both polymorphs have practically the same bond-lengths between the corresponding atoms and practically the same bond-angles, indicating that they have almost identical local environments. The Sr–N bonds, which are indexed with a star (*) in Table 1, ensure the coherence between adjacent planes.

To ensure the chemical stability of both studied polymorphs, their cohesive and formation energies were calculated. The cohesive energy E_{coh} is the energy that is required for the crystal to decompose into free atoms. Therefore, the cohesive energies of α-Sr_2GeN_2 and β-Sr_2GeN_2 were calculated using the following expression:

$$E_{coh} = \frac{1}{5}[E(Sr_2GeN_2) - 2E_a(Sr) - E_a(Ge) - E_a(N_2)], \quad (1)$$

where $E(Sr_2GeN_2)$ represents the total energy of one unit formula of the Sr_2GeN_2 compound, and $E_a(X)$ refers to the total energy of an isolated X atom. The $E_a(X)$ energy was calculated using a cubic box with a large lattice constant. The energy of formation (E_{form}) of a compound is calculated by subtracting the total energies of pure constituent elements in their stable crystal structures from the total energy of the compound. Therefore, the E_{form} of α-Sr_2GeN_2 and β-Sr_2GeN_2 is calculated using the following expression:

$$E_{form} = \frac{1}{5}[E(Sr_2GeN_2) - 2E_s(Sr) - E_s(Ge) - E(N_2)]. \quad (2)$$

In Equation (1), E_s(Sr) and E_s(Ge) denote the total energies per atom of the pure elements Sr and Ge, respectively, in their solid phase, and $E(N_2)$is the total energy of the N_2 molecule. The obtained cohesive and formation energies for α-Sr_2GeN_2 and β-Sr_2GeN_2 are listed in Table 1. Energies for both considered polymorphs are negative, implying that they are both energetically stable and can be synthesized. Furthermore, one can appreciate that E_{coh} and E_{form} energies for the α-Sr_2GeN_2 crystal are slightly lower than those of the β-Sr_2GeN_2 one, implying that the α-Sr_2GeN_2 structure is more stable than the β-Sr_2GeN_2 one. Additionally, the calculated static total energy versus volume (E–V) curves, presented in Figure 2, show that the unit-cell total energy of α-Sr_2GeN_2 is slightly lower than that of the β-Sr_2GeN_2 one, confirming that α-Sr_2GeN_2 structure is more stable than β-Sr_2GeN_2 one. This result is consistent with the fact that synthesis of the α-Sr_2GeN_2 polymorph was not accompanied with the appearance of the β-Sr_2GeN_2 polymorph, while synthesis of the β-Sr_2GeN_2 compound was accompanied with the production of the α-Sr_2GeN_2 polymorph.[24,25]

In order to have insight on the pressure dependence behavior of the structural parameters for the two considered polymorphs, full optimizations of their unit-cell parameters and full relaxations of their atomic positions were performed for fixed pressures in pressure range from 0 to 20 GPa with a step of 5 GPa. Figure 3 displays the pressure dependence of the normalized lattice parameters a/a_0, b/b_0 and c/c_0 and the normalized unit-cell volume V/V_0, where a_0, b_0, c_0 and V_0 are the corresponding values at zero pressure. From Figure 3, it can be seen that the α-Sr_2GeN_2 unit-cell is more compressible along the c-axis than along the a-one, while β-Sr_2GeN_2 unit-cell is less compressible along the b-axis than along the a- and c-ones; a- and c-axes have practically the same compressibility. Further, a look to the pressure dependence of the unit-cell volume, shown in Figure 3, shows that α-Sr_2GeN_2 is slightly less compressible than β-Sr_2GeN_2. The linear compressibility β_X (β_a, β_b and β_c) along the X-axis (a-, b- and c-axes, respectively) has

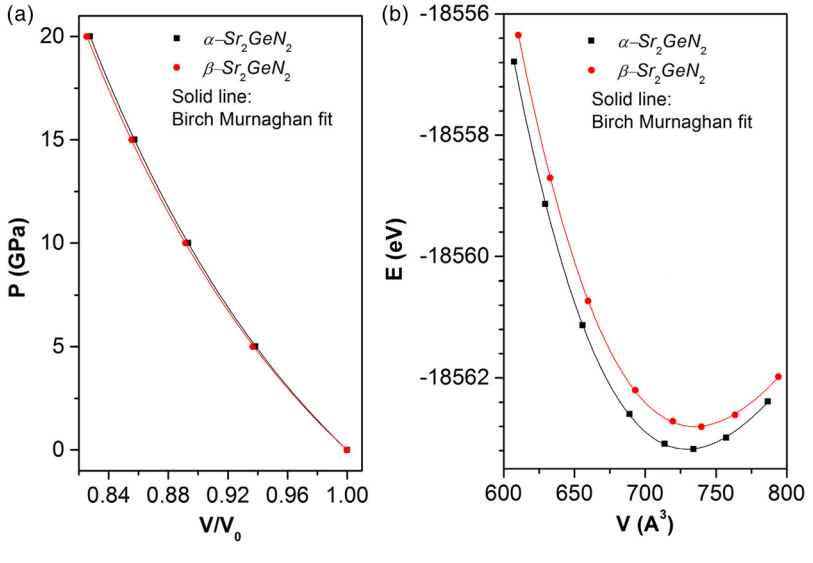

Figure 2. (Colour online) (a) Pressure P versus relative unit-cell volume V/V_0 for α-Sr_2GeN_2 and β-Sr_2GeN_2, (b) Total energy E versus relative unit-cell volume V/V_0 for α-Sr_2GeN_2 and β-Sr_2GeN_2.

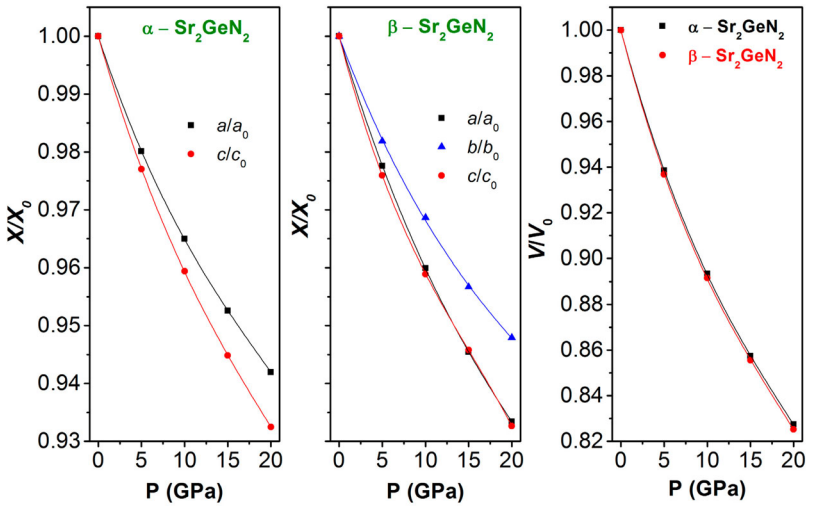

Figure 3. (Colour online) Variation of the normalized lattice parameters ratio; a/a_0, b/b_0 and c/c_0, and the normalized unit-cell volume V/V_0 as a function of hydrostatic pressure P, for the α-Sr_2GeN_2 and β-Sr_2GeN_2 polymorphs. The solid lines are least squares third-order polynomial fits of the data points.

been evaluated from the fit of the lattice parameter X versus pressure data to a third-order polynomial:

$$X/X_0 = 1 + \beta_X P + \sum_{n=2}^{n=3} K_n P^n. \tag{3}$$

The linear compressibilities obtained are $\beta_a = \beta_b = 0.00453\,\mathrm{GPa}^{-1}$ and $\beta_c = 0.00518\,\mathrm{GPa}^{-1}$ for α-Sr_2GeN_2 and $\beta_a = 0.005\mathrm{GPa}^{-1}$, $\beta_b = 0.00399\,\mathrm{GPa}^{-1}$ and $\beta_c = 0.00578\,\mathrm{GPa}^{-1}$ for β-Sr_2GeN_2. The bulk modulus B may be estimated from the linear compressibilities β_a, β_b and β_c via the following relationship: $B = 1/(2\beta_a + \beta_c)$ for α-Sr_2GeN_2 (tetragonal structure) and $B = 1/(\beta_a + \beta_b + \beta_c)$ for β-Sr_2GeN_2 (orthorhombic structure). Moreover, the volume compressibility has been evaluated from the fit of the volume–pressure (V–P) data to a third-order polynomial expression. From Table 1, one can appreciate that the obtained value for the bulk modulus B from the linear compressibilities is in very good agreement with that obtained from the volume compressibility.

One of the more used methods to test the reliability of obtained theoretical results consists of comparing between the numerical values of one property that are calculated using different theoretical procedures. For this issue, the bulk modulus B and its pressure derivative B' were used as test. The bulk modulus values derived from the fitting of the calculated pressure versus unit-cell volume (P–V) data and total energy versus unit-cell volume (E–V) data to some different versions of the equation of state (EOS) [39–42] are compared to that calculated from the elastic constants, linear compressibility and volume compressibility to testify the reliability and accuracy of the present reported results. Figure 2 (a) and 2 (b) presents the fits of the P–V and E–V data to the P–V and E–V Birch–Murnaghan EOSs, respectively, as prototype. One can appreciate the good fit of the first-principles calculated data to the mentioned EOSs. The obtained values of B and B' are reported in Table 1. The

calculated values of the bulk modulus from the EOS fits are in very good agreement with those calculated from the linear and volume compressibilities for both considered materials. These results are good tests of the accuracy of our simulations. To date, no reported experimental or theoretical data in the scientific literature for the bulk moduli of the α-Sr_2GeN_2 and β-Sr_2GeN_2 materials to be compared with our obtained results. According to our results, the bulk modulus B of α-Sr_2GeN_2 is slightly larger than that of β-Sr_2GeN_2 by about 2.0% to 4.0%, revealing that β-Sr_2GeN_2 is slightly more compressible than α-Sr_2GeN_2.

Figure 4 shows the pressure dependence behavior of the relative bond-length d/d_0 of the Ge–N and Sr–N bonds, where d_0 is the equilibrium bond-length at zero pressure. The obtained numerical data are well fitted with a second-order polynomial expression: $d/d_0 = 1 + \alpha P + \beta P^2$. From Figure 4, it can be seen that the Ge–N bond, which belongs to the isolated GeN_2bent units, is stronger than the Sr–N one. The so-called bond stiffness coefficient k is defined by the following relation: $k = 1/|\alpha|$, where α is the first pressure derivative of the bond-length ($d/d_0 = 1 + \alpha P + \beta P^2$), is calculated in order to characterize the stiffness of the existing chemical bonds. The estimated values of the bond stiffness k for the α-Sr_2GeN_2 and β-Sr_2GeN_2 polymorphs are listed in Table 3. One can appreciate that the chemical bonding between two atoms belonging to two adjacent planes is weaker than that between two atoms belonging to the same plane. This behavior could explain the more compressibility of the c-axis (a-axis) in the α-polymorph (β-polymorph) seeing that the stacking is along the c-axis (a-axis) in the α-Sr_2GeN_2 (βSr_2GeN_2) compound. The less compressibility of β-Sr_2GeN_2 along the b-axis compared to a- and c-axes is due to the fact that, statistically, the strongest bond, namely Ge–N1 ($k = 826$ GPa), has greater impact along the b-axis than along the c-one; the angle between the Ge–N1 bond and b-axis is only 14.8° compared to that of 75.2° between the Ge–N1 bond and c-axis.

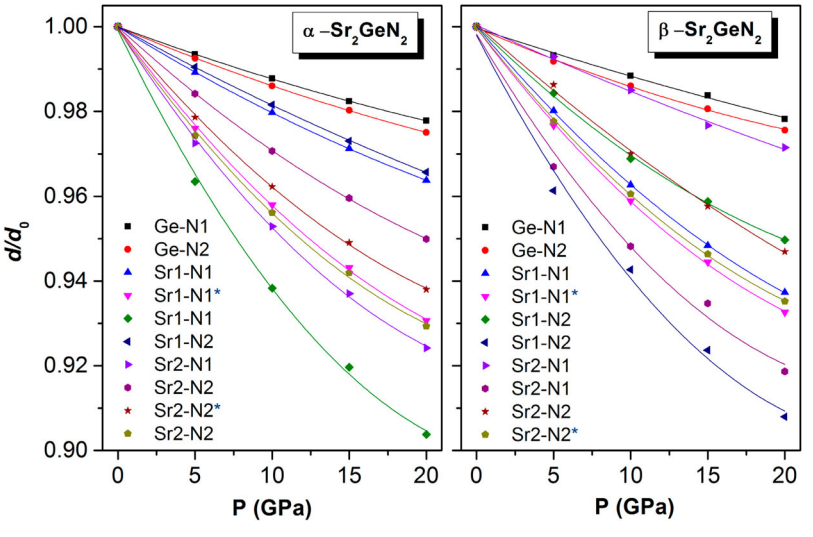

Figure 4. (Colour online) Variation of the relative bond-lengths d/d_0 as a function of hydrostatic pressure P for the α-Sr_2GeN_2 and β-Sr_2GeN_2 compounds. The star (*) indicates the bond between the adjacent planes. The solid lines are least squares second-order polynomial fits of the data points.

Table 3. Calculated bond stiffness (k, in GPa) for some bonds in the α-Sr_2GeN_2 and β-Sr_2GeN_2 compounds.

System	k_{Ge-N1}	k_{Ge-N2}	k_{Sr1-N1}	k_{Sr1-N1}*	k_{Sr1-N1}	k_{Sr1-N2}	k_{Sr2-N1}	k_{Sr2-N2}	k_{Sr2-N2}*	k_{Sr2-N2}
α-Sr_2GeN_2	740.7	653.6	446.4	202.8	134.0	502.5	177.6	300.3	225.7	192.3
β-Sr_2GeN_2	826.4	632.9	230.9	206.6	279.3	142.0	606.1	162.9	306.7	214.1

Note: The star (*) indicates the bond between adjacent planes.

3.2. Elastic properties

3.2.1. Single-crystal elastic constants and related properties

The calculated independent elastic constants C_{ij} and the elastic compliances S_{ij}, which are calculated directly from the C_{ij}, for both studied Sr_2GeN_2 polymorphs are listed in Table 4. The data obtained allow us to highlight the following points.

(1) To be mechanically stable, the C_{ij} of a tetragonal crystal should satisfy the Born–Huang stability criteria [43]:

$$C_{11} > 0, C_{33} > 0, C_{44} > 0, C_{66} > 0, C_{11} - C_{12} > 0, C_{11} + C_{33} - 2C_{13} > 0, 2(C_{11} + C_{12}) + C_{33} + 4C_{13} > 0. \quad (4)$$

The mechanical stability of an orthorhombic crystal requires the following conditions [43]:

$$C_{11} > 0, C_{22} > 0, C_{33} > 0, C_{44} > 0, C_{55} > 0, C_{66} > 0, C_{11} + C_{22} - 2C_{12} > 0, C_{11} + C_{33} - 2C_{13} > 0, C_{22} + C_{33} - 2C_{23} > 0, C_{11} + C_{22} + C_{33} + 2(C_{12} + C_{13} + C_{23}) > 0. \quad (5)$$

The data listed in Table 4 demonstrate that the C_{ij} of both examined polymorphs satisfy the above-mentioned criteria. This implies that the examined polymorphs α-Sr_2GeN_2 and β-Sr_2GeN_2 are mechanically stable.

(1) C_{11} is slightly higher than C_{33} in the α-Sr_2GeN_2 crystal, which means that the resistance against the applied stress along the [100] crystallographic direction is slightly higher

Table 4. Calculated independent elastic constants (C_{ij}, in GPa) and elastic compliance (S_{ij}, in GPa^{-1}) for the α-Sr_2GeN_2 and β-Sr_2GeN_2 single-crystals.

α-Sr_2GeN_2		β-Sr_2GeN_2	
C_{ij}	S_{ij}	C_{ij}	S_{ij}
$C_{11} = 124.8$	$S_{11} = 0.0097517$	$C_{11} = 123.2$	$S_{11} = 0.0092388$
$C_{33} = 123.5$	$S_{33} = 0.0090089$	$C_{22} = 134.4$	$S_{22} = 0.0088889$
$C_{44} = 36.7$	$S_{44} = 0.0272196$	$C_{33} = 127.9$	$S_{33} = 0.0088393$
$C_{66} = 40.9$	$S_{66} = 0.0244564$	$C_{44} = 40.0$	$S_{44} = 0.0250226$
$C_{12} = 48.4$	$S_{12} = -0.0033363$	$C_{55} = 25.2$	$S_{55} = 0.0396926$
$C_{13} = 32.7$	$S_{13} = -0.0017018$	$C_{66} = 40.6$	$S_{66} = 0.0246356$
		$C_{12} = 41.3$	$S_{12} = -0.0024495$
		$C_{13} = 28.6$	$S_{13} = -0.0012805$
		$C_{23} = 40.9$	$S_{23} = -0.0022928$

than the resistance to the applied stress along the [001] one. This suggests that the chemical bonding between nearest neighbors along the [100] direction is slightly stronger than those along the [001] one. In the β-Sr_2GeN_2 crystal, C_{22} is slightly higher than C_{11} and C_{33}, implying that the resistance against the external applied stress along the [010] direction is slightly higher than that against the external applied stress along the [100] and [001] directions. This result suggests that the inter-atomic interactions along the [010] crystallographic direction are slightly stronger than those along the [100] and [001] ones. These results are in concordance with those obtained from the pressure dependence behavior of the lattice parameters and chemical bond-lengths, which have been already discussed in Section 3.1.

(2) It is important to evaluate the sound velocity in a crystal because they are related to some physical properties of the material such as its thermal conductivity. Single-crystal elastic wave velocities propagating in different crystallographic directions can be predicted from the resolution of the Christoffel equation [44]:

$$(C_{ijkl}n_jn_k - \rho V^2\delta_{il})u_l = 0. \tag{6}$$

Here, C_{ijkl} are the components of the elastic constant tensor in the full (4-index) notation, $\vec{n}$ is the wave propagation direction, ρ is the mass density of the propagating medium, V is the sound-wave velocity and $\vec{u}$ is the sound-wave polarization. The pure longitudinal (L) and transverse (T) wave velocities propagating along the [100], [010] and [001] crystallographic directions in an orthorhombic system are given by the following expressions:

$$\begin{array}{lll} V_L^{[100]} = \sqrt{C_{11}/\rho}; & V_{T1}^{[100]} = \sqrt{C_{66}/\rho}; & V_{T2}^{[100]} = \sqrt{C_{55}/\rho}, \\ V_L^{[010]} = \sqrt{C_{22}/\rho}; & V_{T1}^{[010]} = \sqrt{C_{66}/\rho}; & V_{T2}^{[010]} = \sqrt{C_{44}/\rho}, \\ V_L^{[001]} = \sqrt{C_{33}/\rho}; & V_{T1}^{[001]} = \sqrt{C_{55}/\rho}; & V_{T2}^{[001]} = \sqrt{C_{44}/\rho}. \end{array} \tag{7}$$

The pure L and T sound-wave velocities propagating along the [100] (or [010]), [001] and [110] crystallographic directions of a tetragonal system are given by the following expressions:

$$\begin{aligned} &V_L^{[100]} = \sqrt{C_{11}/\rho};\ V_{T1}^{[100]} = \sqrt{C_{66}/\rho};\ V_{T2}^{[100]} = \sqrt{C_{44}/\rho}, \\ &V_L^{[001]} = \sqrt{C_{33}/\rho};\ V_{T1}^{[001]} = V_{T2}^{[001]} = \sqrt{C_{44}/\rho}, \\ &V_L^{[110]} = \sqrt{(C_{11}+C_{12}+2C_{66})/2\rho};\ V_{T1}^{[110]} = \sqrt{(C_{11}-C_{12})/2\rho}\, V_{T2}^{[110]} = \sqrt{C_{44}/\rho}. \end{aligned} \tag{8}$$

The calculated elastic wave velocities along the above-mentioned crystallographic directions for the α-Sr_2GeN_2 and β-Sr_2GeN_2 polymorphs are listed in Table 5. One can

Table 5. Elastic wave velocities (in m/s) for some different propagating crystallographic directions for the α-Sr_2GeN_2 and β-Sr_2GeN_2 crystals.

α-Sr_2GeN_2	v_L^{100}	v_{T1}^{100}	v_{T2}^{100}	v_L^{001}	v_{T1}^{001}	v_{T2}^{001}	v_L^{110}	v_{T1}^{110}	v_{T2}^{110}
	5000.7	2862.1	2713.0	4971.4	2713.0	2713.0	5054.2	2766.5	2713.0
β-Sr_2GeN_2	v_L^{100}	v_{T1}^{100}	v_{T2}^{100}	v_L^{010}	v_{T1}^{010}	v_{T2}^{010}	v_L^{001}	v_{T1}^{001}	v_{T2}^{001}
	4986.1	2862.6	2255.2	5209.3	2862.6	2840.4	5080.7	2255.2	2840.4

appreciate that the longitudinal sound-wave velocities have almost equal values for both considered compounds (~5000 m/s) and they are larger than the transverse ones.

Figure 5 shows the variations of the elastic constants C_{ij} versus hydrostatic pressure. One can observe that C_{11}, C_{33} and $C_{12,}$ especially C_{33}, for α-Sr_2GeN_2 are highly sensitive to pressure variations than other constants.The C_{44} remains almost invariable to the pressure variations. For β-Sr_2GeN_2, C_{11}, C_{22}, C_{33} and C_{23}, especially C_{11}, are the highly sensitive to pressure variations than other constants. The C_{44}, C_{55} and C_{66} remain almost invariable to pressure variations. Under pressure, for the tetragonal crystal, the mechanical stability requires that the elastic constants satisfy the following stability criteria [45,46]:

$$C_{11} - P > 0,\ C_{33} - P > 0,\ C_{44} - P > 0 \text{ and } C_{66} - P > 0,$$
$$C_{11} - C_{12} - 2P > 0,\ C_{11} + C_{33} - 2C_{13} - 4P > 0,\ 2(C_{11} + C_{12}) + C_{33} + 4C_{13} + 3P > 0. \quad (9)$$

For the orthorhombic crystal, the required criteria are as follows [45,46]:

$$C_{11} - P > 0,\ C_{22} - P > 0,\ C_{33} - P > 0,\ C_{44} - P > 0,\ C_{55} - P > 0,\ C_{66} - P > 0,$$
$$C_{11} + C_{22} - 2C_{12} - 4P > 0,\ C_{11} + C_{33} - 2C_{13} - 4P > 0,\ C_{22} + C_{33} - 2C_{23} - 4P > 0,$$
$$C_{11} + C_{22} + C_{33} + 2(C_{12} + C_{13} + C_{23}) + 3P > 0. \quad (10)$$

Both investigated polymorphs satisfy the required criteria for mechanical stability in the considered pressure range.

3.2.2. Elastic moduli and related properties for polycrystalline aggregates

Generally, it is difficult to synthetize materials in single-crystal form, and in this case, the elastic constants C_{ij} cannot be measured. In the polycrystalline aggregates form, only

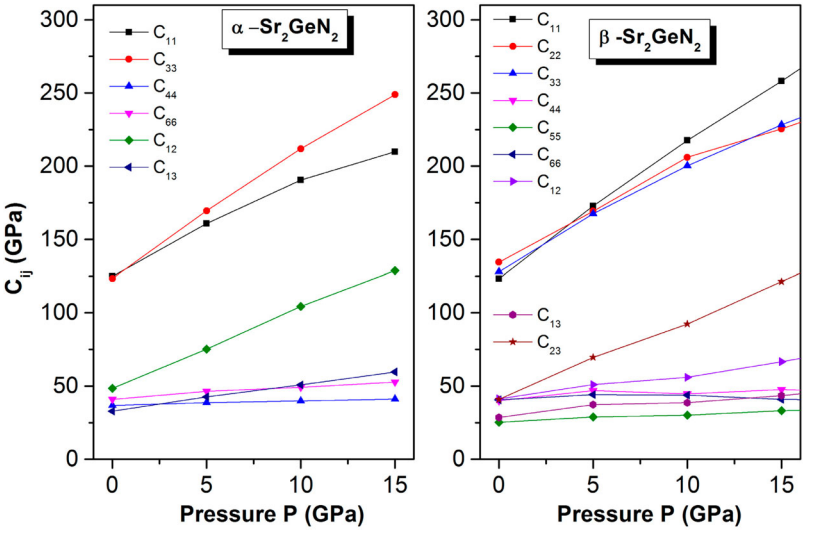

Figure 5. (Colour online) Variation of the elastic constants C_{ij} for the α-Sr_2GeN_2 and β-Sr_2GeN_2 as a function of pressure.

the isotropic polycrystalline elastic moduli can be measured. Theoretically, polycrystalline elastic moduli such as the bulk modulus B (which represents the resistance of a solid against volume change under hydrostatic pressure), shear modulus G (which represents the resistance of a solid to shape change caused by a shearing force) and Young's modulus E (which represents the resistance of a solid against uniaxial stress) can be derived from the calculated single-crystal elastic constants C_{ij} using some approximations. In the case of randomly oriented polycrystals, one may evaluate aggregate average elastic properties based on additional hypotheses such as isostress named as Reuss [35] or isostrain named as Voigt [36] states (subscripted, respectively, R and V in the following). The general expressions for the Voigt and Reuss approaches for bulk and shear moduli are expressed as follows [35,36]:

$$B_V = (1/9)[C_{11} + C_{22} + C_{33} + 2(C_{12} + C_{13} + C_{23})], \tag{11}$$

$$G_V = (1/15)[C_{11} + C_{22} + C_{33} + 3(C_{44} + C_{55} + C_{66}) - (C_{12} + C_{13} + C_{23})], \tag{12}$$

$$1/B_R = (S_{11} + S_{22} + S_{33}) + 2(S_{12} + S_{23} + S_{13}), \tag{13}$$

$$1/G_R = (4/15)[(S_{11} + S_{22} + S_{33}) - (4/15)(S_{12} + S_{13} + S_{23}) + (1/5)(S_{44} + S_{55} + S_{66})]. \tag{14}$$

Here, the S_{ij} are the components of the compliance matrix **S**, which is related to the elastic constant matrix **C** by the following relationship: $\mathbf{S} = \mathbf{C}^{-1}$. Hill [37] has demonstrated that the arithmetic mean of the two above-mentioned limits – Voigt and Reuss – are the best effective polycrystalline elastic moduli (Hill's approximation). In the Hill's approximation the polycrystalline bulk (B_H) and shear (G_H) moduli are given by the following expressions:

$$B_H = \frac{B_V + B_R}{2},\ G_H = \frac{G_V + G_R}{2}. \tag{15}$$

The Young's modulus E and Poisson's ratio σ, which is defined as the ratio of transverse strain (normal to the applied stress) to the longitudinal strain (in the direction of the applied stress), can be computed from the Hill's values of B and G through the following relations:

$$E = \frac{9B_H G_H}{3B_H + G_H},\ \sigma = \frac{3B_H - 2G_H}{2(3B_H + G_H)}. \tag{16}$$

Using the above-mentioned relations, the calculated bulk modulus, shear modulus, Young's modulus and Poisson's ratio are summarized in Table 6. From these obtained results, one can make the following conclusions.

Table 6. Calculated bulk modulus (B_H, in GPa), shear modulus (G_H, in GPa), Yong's modulus (E_H, in GPa), B/G ratio and Poisson's ratio (σ_H, dimensionless) for the α-Sr_2GeN_2 and β-Sr_2GeN_2 polycrystals. The subscript V, R and H stand to Voigt, Reuss and Hill approximations.

System	B_V	B_R	B_H	G_V	G_R	G_H	E_H	B/G	σ_H
α-Sr_2GeN_2	66.75	66.52	66.64	40.15	39.717	39.930	99.850	1.67	0.250
β-Sr_2GeN_2	67.43	67.02	67.224	39.47	37.50	38.480	96.95	1.75	0.260

(1) The polycrystalline elastic moduli calculated for both Sr_2GeN_2 polymorphs are almost equal, indicating the resemblance of their mechanical properties.
(2) Calculated bulk modulus from the single-crystal elastic constants C_{ij} is in good agreement with that calculated from the EOS fits for both considered polymorphs. This serves to give an indication of the reliability and accuracy of our predicted elastic constants. The calculated bulk modulus value for both compounds is smaller than 100 GPa; so these two compounds can be classified as a relatively soft material.
(3) The Poison's ration σ is often used to reflect the stability of a crystal against shear and provides information about the nature of the bonding forces. The value of $\sigma$for covalent materials is small ($\sigma = 0.1$), whereas for ionic materials, a typical value for σ is 0.25. [28,47] The calculated σ for both crystals are almost equal:$\sigma = 0.25$ for α-Sr_2GeN_2 and $\sigma = 0.26$ for β-Sr_2GeN_2. These values indicate that a considerable ionic contribution in the inter-atomic bonding should be assumed in these crystals. On the other hand, for covalent and ionic materials, the typical relations between bulk and shear modulus are $G \approx 1.1\ B$ and $G \approx 0.6\ B$, respectively. We found that $G \approx 0.6\ B$ for both crystals, which also suggests the dominance of the ionic nature in the two considered compounds.
(4) To know if a material has a brittle or a ductile behavior, Pugh [48] has proposed a simple empirical relationship between the bulk modulus B and shear modulus G. The shear modulus G represents the resistance to plastic deformation, while B represents their resistance to fracture. Therefore, a high B/G ratio is associated with ductility, whereas a low value corresponds to brittle nature. The critical value that separates ductile and brittle materials is around 1.75 [48]; that is, if $B/G > 1.75$, the material behaves in a ductile manner, otherwise, the material behaves in a brittle manner. For β-Sr_2GeN_2, the B/G ratio is exactly equal to the critical value;$B = 1.75$; therefore, its mechanical properties are intermediate between those of a ductile material and a brittle material. For α-Sr_2GeN_2, the B/G ratio is slightly lower than the critical value 1.75; therefore, this compound is considered somewhat a brittle material.
(5) Within the Debye model, the Debye temperature $\theta_D$is one of the fundamental parameters of solids; it is closely correlated with many physical properties, such as heat capacity, melting temperature, thermal expansion, elastic constants and so on. The $\theta_D$is the highest temperature that can be achieved due to a single normal vibration and then it is used to distinguish between high- and low-temperature regions for a solid. The θ_D can be numerically estimated from the average sound-wave velocity V_m through the following relationship [49]:

$$\theta_D = \frac{h}{K_B}\left[\frac{3n}{4\pi}\left(\frac{N_A\rho}{M}\right)\right]^{1/3} V_m. \tag{17}$$

where h is the Planck's constant, k_B is the Boltzmann's constant, N_A is the Avogadro's number, ρ is the mass density, M is the molecular weight and n is the number of atoms in the molecule. The average sound-wave velocity V_m in the polycrystalline materials can be computed using the following expression:

$$V_m = \left[\frac{1}{3}\left(\frac{2}{V_t^3} + \frac{1}{V_l^3}\right)\right]^{-1/3} \tag{18}$$

Here, V_l and V_t are the longitudinal and transverse sound-wave velocities in the polycrystalline material, respectively, which can be calculated from the Navier's equation [50]:

$$V_t = \left(\frac{G}{\rho}\right)^{1/2},\ V_l = \left(\frac{3B+4G}{3\rho}\right)^{1/2}. \tag{19}$$

The calculated sound-wave velocities (V_l,V_t andV_m) and Debye temperature (θ_D) for the polycrystalline α-Sr_2GeN_2 and β-Sr_2GeN_2 compounds are listed in Table 7. One can see from this table that the values of ρ,V_l, V_t, V_m and θ_D of α-Sr_2GeN_2 are slightly larger than those of β-Sr_2GeN_2.

3.2.3. Elastic anisotropy

Crystal anisotropy reflects the difference between the atomic arrangements along different directions. Crystal anisotropy has an important implication in engineering science as well as in crystal physics; for example, microcracks can easily induced in materials having significant anisotropy of the thermal expansion coefficient as well as elastic anisotropy.[51] Furthermore, recent research demonstrates that the elastic anisotropy has a significant influence on the nanoscale precursor textures in alloys.[52] Therefore, it is necessary and significant to properly describe the elastic anisotropy of solids in order to understand this property and consequently to find mechanisms that will improve their resistance to microcracks. Elastic anisotropy behavior of a crystal can be sufficiently and completely described by plotting three-dimensional (3D) representation of directional dependence of its elastic moduli. To visualize the elastic anisotropy extent of the two considered crystals, 3D closed surfaces illustrating the dependence of the Young's modulus E and linear compressibility β on the crystallographic directions are plotted. In tetragonal and orthorhombic crystals, the 3D closed surfaces for E and β are described by the following relationships [53]:

$$\text{Tetragonal:}\begin{cases}\dfrac{1}{E} = (l_1^4 + l_2^4)S_{11} + l_3^4 S_{33} + 2l_1^2 l_2^2 S_{12} + 2(l_1^2 l_3^2 + 2l_2^2 l_3^2)S_{13} + (l_2^2 l_3^2 + l_1^2 l_3^2)S_{44} + l_1^2 l_2^2 S_{66} \\ \beta = (S_{11} + S_{12} + S_{13}) - (S_{11} + S_{12} - S_{13} - S_{33})l_3^2\end{cases}. \tag{20}$$

$$\text{Orthorombic:}\begin{cases}\dfrac{1}{E} = l_1^4 S_{11} + l_2^4 S_{22} + l_3^4 S_{33} + 2l_1^2 l_2^2 S_{12} + 2l_1^2 l_3^2 S_{13} + 2l_2^2 l_3^2 S_{23} + l_2^2 l_3^2 S_{44} + l_1^2 l_3^2 S_{55} \\ +l_1^2 l_2^2 S_{66} \ = (S_{11} + S_{12} + S_{13})l_1^2 + (S_{12} + S_{22} + S_{23})l_2^2 + (S_{13} + S_{23} + S_{33})l_3^2.\end{cases} \tag{21}$$

Here, l_1, $l_2$and l_3 are the directional cosines with respect to the *x*-, *y*- and *z*-axes, respectively, and the S_{ij} stand to the elastic compliance constants that can be obtained through

Table 7. Molecular weight (M, in g/mol), density (ρ, in g/cm^3), transverse, longitudinal and average sound velocities (V_l, V_t andV_m, respectively, in m/s) and the Debye temperatures (θ_D, in K) for the α-Sr_2GeN_2 and β-Sr_2GeN_2 compounds.

Compound	M	P	V_l	V_t	V_m	θ_D
α-Sr_2GeN_2	275.844	4.9915	2828.4	4900.7	3140.2	354.4
β-Sr_2GeN_2	275.844	4.9534	2787.3	4891.7	3097.9	348.8

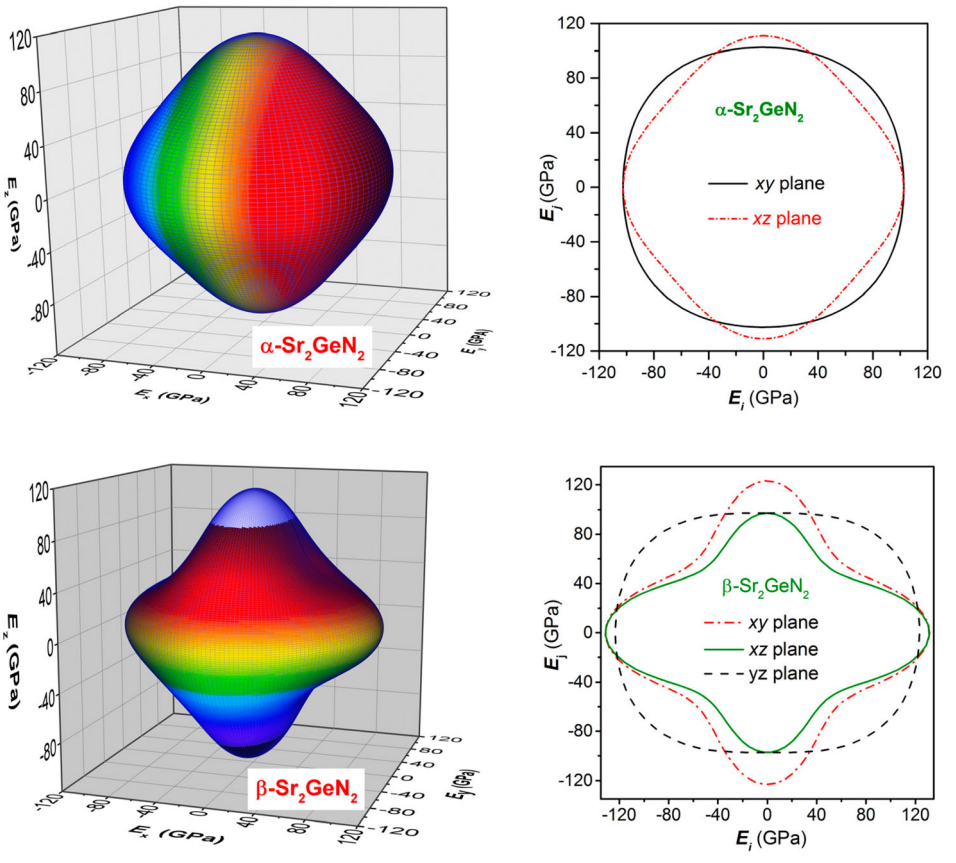

Figure 6. (Colour online) Directional dependence of the Young's modulus and its cross sections in different planes for α-Sr_2GeN_2 and β-Sr_2GeN_2 crystals. The distance between zero and any point on the surface is equal to the Young's modulus in that direction.

an inversion of the elastic constant tensor. In a 3D-representation, the distance from the origin of the system of coordinates to this surface gives the value of the represented elastic modulus in a given direction. Thus, in a 3D representation, a perfectly isotropic system would exhibit a spherical shape, and the degree of deviation of the 3D surface from spherical shape reveals the extent of the elastic anisotropy. Figure 6 and Figure 7 illustrates 3D representation of the directional dependence of the Young's modulus *E* (linear compressibility *β*) together with its cross section in the *xy*, *xz* and *yz* crystallographic planes for α-Sr_2GeN_2 and β-Sr_2GeN_2 crystals. From Figure 6 and Figure 7, one can observe the appreciable deviation of the 3-D representation of the Young's modulus (linear compressibility) from the spherical shape in both studied crystals, suggesting that α-Sr_2GeN_2 and β-Sr_2GeN_2 crystals exhibit a pronounced elastic anisotropy.

3.3. Thermodynamic properties

Investigation of the thermodynamic properties of solids at high pressure and high temperature is an interesting topic in the condensed matter physics. Here, we applied the quasi-

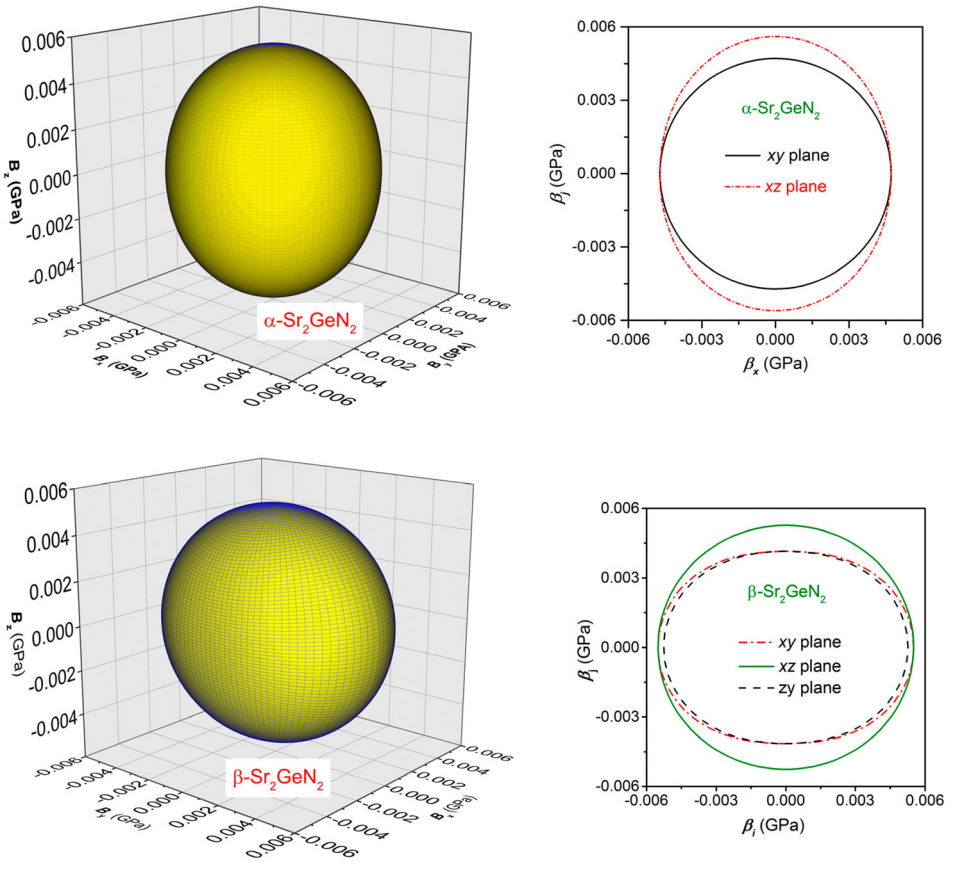

Figure 7. (Colour online) Directional dependence of the linear compressibility and its cross sections in different planes for α-Sr_2GeN_2 and β-Sr_2GeN_2 crystals. The distance between zero and any point on the surface is equal to the linear compressibility β in that direction.

harmonic Debye approximation [37] to investigate the thermodynamic properties of the α-Sr_2GeN_2 and β-Sr_2GeN_2 compounds. The thermal properties are determined in the temperature range from 0 to 900 K at some fixed pressures ($P = 0$, 5, 10, 15 GPa).

The heat capacity of a crystal does not only provide essential information on its vibrational properties, but it is also mandatory for many applications. Temperature dependence of the constant volume heat capacity C_V at some fixed pressures is shown in Figure 8. From this figure, one can see the sharp increase of C_V in the temperature range from 0 up to ~200 K and at high temperature, the C_V tends to a constant value (997.7 J mol^{-1} K^{-1}), the so-called Dulong-Petit limit. At 300 K and zero pressure, $C_V = 936.04$ J mol^{-1} K^{-1} for α-Sr2GeN_2 and 935.37 J mol^{-1} K^{-1} for β-Sr_2GeN_2.

The thermal expansion coefficient α reflects the temperature dependence of the volume at constant pressure. Figure 9 shows the evolution of the thermal expansion coefficient α with temperatures at some different fixed pressures. From this figure, we can see that the thermal expansion increases sharply with temperature in the temperature range from 0 K up to ~200 K, especially at zero pressure, then for temperature higher than 200 K, the increase becomes slowly and gradually approaches a linear increase. For a given

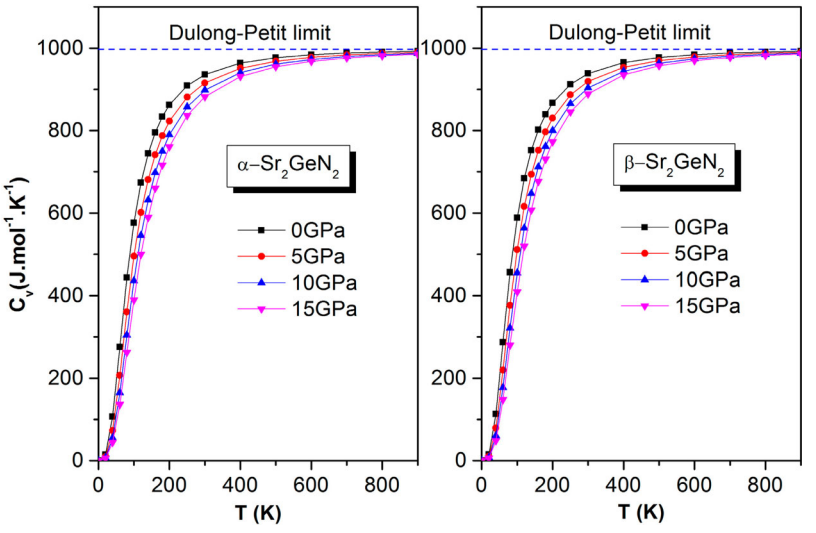

Figure 8. (Colour online) The heat capacity versus temperature at different pressures for the α-Sr2GeN$_2$ and β-Sr$_2$GeN$_2$.

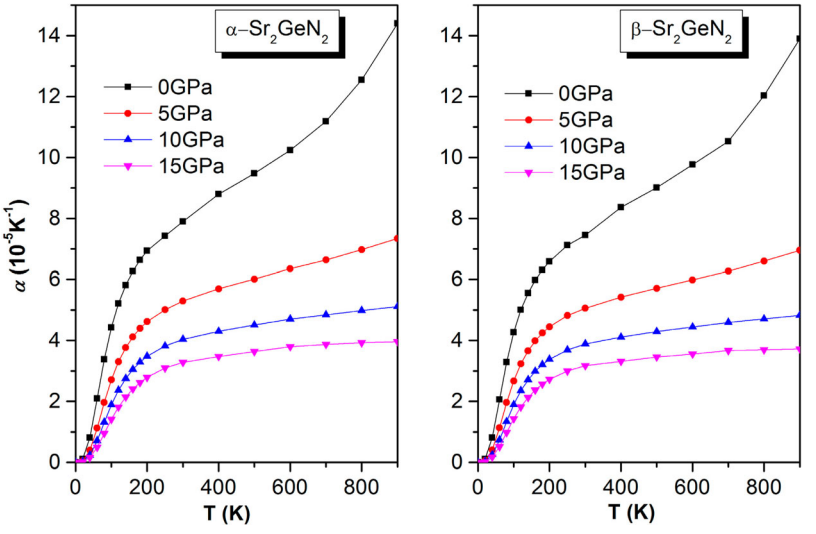

Figure 9. (Colour online) The thermal expansion coefficient versus temperature at different pressures for the α-Sr2GeN$_2$ and β-Sr$_2$GeN$_2$.

temperature, α decreases drastically with the increase of pressure. At zero pressure and 300 K, $\alpha = 7.91242 \times 10^{-5}$ K^{-1} for α-Sr2GeN$_2$ and 7.42234×10^{-5} K^{-1} for β-Sr$_2$GeN$_2$.

Figure 10 shows temperature dependence of the Debye temperature θ_D at some fixed pressures. At fixed pressure, Debye temperature decreases with increasing temperature and at fixed temperature, θ_D increases with increasing pressure, indicating the change of the vibration frequency of particles under pressure and temperature effects. From Figure 10, one can observe that as the pressure goes higher, the decreasing slope of θ_D with temperature becomes smaller; the high pressure suppresses the temperature

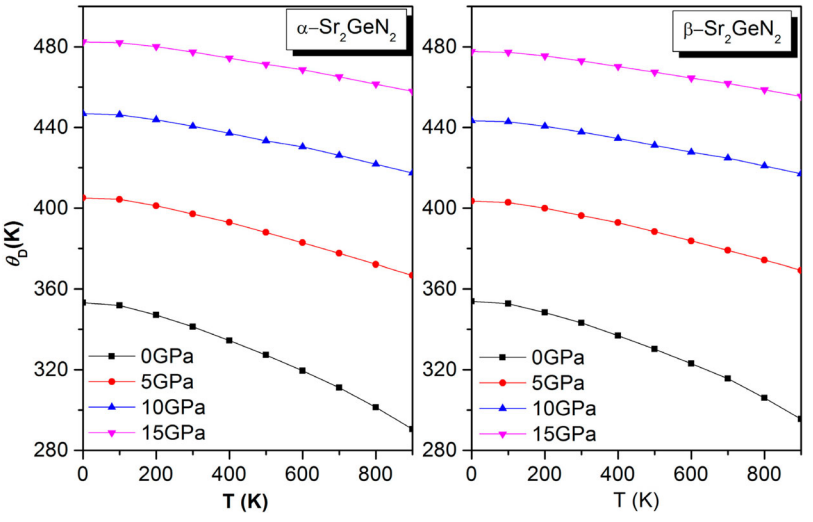

Figure 10. (Colour online) The Debye temperature θ_D versus temperature at different pressures for the α-Sr2GeN$_2$ and β-Sr$_2$GeN$_2$.

effect. At zero pressure and zero temperature, Debye temperatures for α-Sr$_2$GeN$_2$ and β-Sr$_2$GeN$_2$ are 353.2 and 353.9 K, respectively. It is worth to note here that the value of θ_D calculated using the Debye model is in good agreement with that calculated from the sound velocities (354.43 and 348.76 K, respectively).

Figure 11 depicts the variation of bulk modulus versus temperature at some given pressures. The bulk modulus *B* decreases with increasing temperature at a given pressure and increases with pressure at a given temperature.

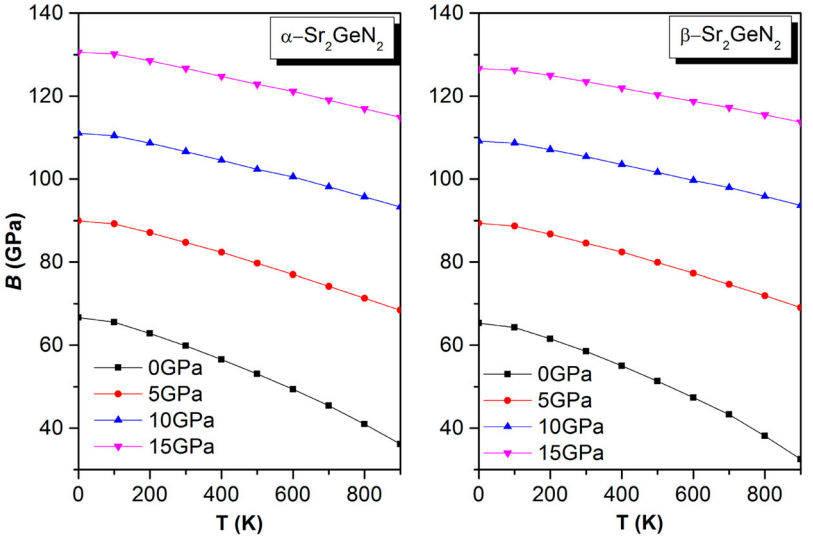

Figure 11. (Colour online) The bulk modulus *B* versus temperature at different pressures for the α-Sr2GeN$_2$ and β-Sr$_2$GeN$_2$.

4. Conclusion

We have reported the results of first-principle calculations of the structural, elastic and thermodynamic properties of the α and β polymorphs of the ternary nitrides Sr_2GeN_2. The optimized structural parameters, including lattice parameters, atomic positions and inter-atomic bond-lengths, reproduce the available experimental data. The calculated cohesive energy and formation enthalpy demonstrate that both examined polymorphs are energetically stable. The calculated pressure dependence of the lattice parameters shows that α-Sr_2GeN_2 is slightly more compressible along the *c*-axis than along the *a*-axis, whereas β-Sr_2GeN_2 is slightly more compressible along the *c*-axis and *a*-axis than along the *b*-axis. Pressure dependence of the bond-lengths reveals that chemical bonding between neighbors inside the stacking planes is stronger than those between adjacent planes. We have evaluated the single-crystal and polycrystalline elastic moduli and related properties. The calculated bulk modulus from the single-elastic constants is in good agreement with those estimated from different EOS fits. This serves to give an indication of the accuracy of our predicted elastic constants. The two examined polymorphs have relatively a small bulk modulus ($B < 100$ GPa); so they are classified as a relatively soft material. According to Pugh's criterion, both phases are intermediate between ductile and brittle materials. The investigated crystals exhibit a strong elastic anisotropy. Using the quasi-harmonic Debye model, temperature dependences of the heat capacity, thermal expansion, Debye temperature and bulk modulus at some fixed pressures are predicted in temperature range from of 0 to 900 K. The calculated Debye temperature at zero pressure and zero temperature through this model is in good agreement with that calculated from the elastic constants. To the best of our knowledge, there are no previous reports on the elastic and thermodynamic properties; so, we hope that future experimental and theoretical investigations of these materials will testify our present reported results.

References

[1] Matsuoka T. Progress in nitride semiconductors from GaN to InN-MOVPE growth and characteristics. Superlattice Microstruct. 2005;37:19–32.
[2] Lam KT, Chang PC, Chang SJ, et al. Nitride-based photodetectors with unactivated Mg-doped GaN cap layer. Sens Actuators A. 2008;143:191–195.
[3] Yan H, Chen Y, Xu S. Synthesis of graphitic carbon nitride by directly heating sulfuric acid treated melamine for enhanced photocatalytic H2 production from water under visible light. Int J Hydrogen Energy. 2012;37:125–133.
[4] Wen Z, Wang K, Chen L, Xie J. A new ternary composite lithium silicon nitride as anode material for lithium ion batteries. Electrochem Commun. 2006;8:1349–1352.
[5] Chen XZ, Eick HA. J. A new quaternary nitride, Li3Ba2NbN4. Solid State Chem. 1994;113:362–366.
[6] Herle PS, Vasanthacharya NY, Hegde MS, Gopalakrishnan J. Synthesis of new transition metal nitrides, MWN2 (M = Mn, Co, Ni). J. Alloys Compd. 1995;217:22–24.
[7] Cheviré F, DiSalvo Francis J. A new ternary nitride La2GaN3: synthesis and crystal structure. J. Alloys Compd. 2008;457:372–375.
[8] Park DG, Dong Y, DiSalvo FJ. Sr(Mg3Ge)N4 and Sr(Mg2Ga2)N4: New isostructural Mg-containing quaternary nitrides with nitridometallate anions of View the MathML source[(Mg3Ge)N4]2−∞3 and View the MathML source[(Mg2Ga2)N4]2−∞3 in a 3D-network structure. Solid State Sci. 2008;10:1846–1852.

[9] Yamane H, Morito H. Ba4Mg[Si2N6], Ba3Ca2[Si2N6] and Ba1.6Sr3.4[Si2N6] – quaternary barium alkaline-earth silicon nitrides containing isolated nitridosilicate anions of [Si2N6]10–. J. Alloys Compd. 2013;555:320–324.
[10] Park DG, Gál ZA, DiSalvo FJ. Synthesis and structure of Li4Sr3Ge2N6: a new quaternary nitride containing Ge2N610– anions. J. Solid State Chem. 2003;172:166–170.
[11] Pagano S, Lupart S, Schmiechen S, Schnick W. Li4Ca3Si2N6 and Li4Sr3Si2N6 - quaternary lithium nitridosilicates with isolated [Si2N6]10- Ions. Zeitschrift fur Anorganische und Allgemeine Chemie. 2010;636:1907–1909.
[12] Yamane H, Morito H. J. Alloys Compd. 2013;555:320.
[13] Ghazai AJ, Aziz WJ, Abu Hassan H, Hassan Z. Quaternary n-Al0.08In0.08Ga0.84N/p-Si-based solar cell. Superlattice Microstruct. 2012;51:480–485.
[14] Jetter M, Wächter C, Meyer A, Feneberg M, Thonke K, Michler P. Quaternary AlxInyGa1–x–yN layers deposited by pulsed metal-organic vapor-phase epitaxy for high efficiency light emission. J Cryst Growth. 2011;315:254–257.
[15] Kyono T, Hirayama H, Akita K, Nakamura T. Effects of in composition on ultraviolet emission efficiency in quaternary InAlGaN light-emitting diodes on freestanding GaN substrates and sapphire substrates. J Appl Phys. 2005;98:113514 (1-8).
[16] Park DG, Dong Y, DiSalvo FJ. Solid State Sci. 2008;10:1846–1852.
[17] Bailey MS, DiSalvo Francis J. Synthesis and crystal structure of LiCaGaN2. J. Alloys Compd. 2006;417:50–54.
[18] Chen XZ, Eick HA. Synthesis and structure of two new quaternary nitrides: Li3Sr2MN4(M=Nb, Ta). J Solid State Chem. 1997;130:1–8.
[19] Park DG, Gál ZA, DiSalvo FJ. Synthesis and structure of LiSrGaN2: a new quaternary nitride with interpenetrating two-dimensional networks. J Alloys Compd. 2003;353:107–113.
[20] Chen XZ, Ward DL, Eick HA. Synthesis and structure of Li3Ba2TaN4. J Alloys Compd. 1994;206:129–132.
[21] Bowman A, Smith RI, Gregory DH. Synthesis and structure of the ternary and quaternary strontium nitride halides, Sr2N(X, X′) (X, X′=Cl, Br, I). J Solid State Chem. 2006;179:130–139.
[22] Pust P, Pagano S, Schnick W. Organic chemistry. Eur J Inorg Chem. 2013;7:1157–1160.
[23] Park DG, Di Salvo FJ. Synthesis and crystal structure of a new quaternary nitride, Li4Ca13Ge6N18. Bull Korean Chem Soc. 2012;33:1759–1761.
[24] Clarke SJ, Kowach GR, DiSalvo FJ. Synthesis and Structure of Two New Strontium Germanium Nitrides: Sr3Ge2N2 and Sr2GeN2. Inorg Chem. 1996;35:7009–7012.
[25] Park DG, Gál Z, DiSalvo FJ. Synthesis and structure of a second polymorph of strontium germanium nitride: β-Sr2GeN2. Bull Korean Chem Soc. 2005;26:786–790.
[26] Alahmed Zeyad A, Reshak Ali H. DFT calculation of the electronic structure and optical properties of two strontium germanium nitrides: α-Sr2GeN2 and β-Sr2GeN2. J Alloys Compd. 2013;559:181–187.
[27] Gleize H, Demangeot F, Frandon J, et al. Phonons in a strained hexagonal GaN–AlN superlattice. Appl Phys Lett. 1999;74:703 (1-3).
[28] Bouhemadou A, Uğur G, Uğur Ş, et al. Elastic and thermodynamic properties of ZnSc2S4 and CdSc2S4 compounds under pressure and temperature effects. Comput Mat Sci 2013;70:107–113.
[29] Bouhemadou A, Khenata R, Kharoubi M, et al. FP-APW + lo calculations of the elastic properties in zinc-blende III-P compounds under pressure effects. Comput Mat Sci. 2009;45:474–479.
[30] Clark SJ, Segall MD, Pickard CJ, et al. First principles methods using CASTEP. Zeitschrift fuer Kristallographie. 2005;220:567–570.
[31] Perdew JP, Ruzsinszky A, Csonka GI, et al. Phys Rev Lett. 2008;100:136406-1–4.
[32] Vanderbilt D. Soft self-consistent pseudopotentials in a generalized eigenvalue formalism. Phys Rev B. 1990;41:7892-1–4.
[33] Monkhorst HJ, Pack JD. Special points for Brillouin-zone integrations. Phys Rev B. 1976;13:5188-1–5.
[34] Fischer TH, Almlof J. General methods for geometry and wave function optimization. J Phys Chem. 1992;96:9768–9774.

[35] Reuss A, Berechnung der Fließgrenze von Mischkristallen auf Grund der Plastizitätsbedingung für Einkristalle (Calculation of the yield strength of solid solutions based on the plasticity condition of single crystals). Angew Z. Math Mech. 1929;9:49–58.
[36] Voigt W. Lehrbuch der Kristallphysik. Leipzig: Taubner; 1928.
[37] Hill R. The elastic behavior of a crystalline aggregate. Proc Phys Soc Lond Sect A. 1952;65:349–354.
[38] Blanco MA, Francisco E, Luaña V. GIBBS: isothermal-isobaric thermodynamics of solids from energy curves using a quasi-harmonic Debye model. Comput Phys Commun. 2004;158:57–72.
[39] Birch F. Finite strain isotherm and velocities for single crystal and polycrystalline NaCl at high pressure and 300K. J Geophys Res B. 1978;83:1257–1268.
[40] Murnaghan FD. The compressibility of media under extreme pressure, Proc Natl Acad Sci USA. 1944;30:244–247.
[41] Birch F. Finite elastic strain of cubic crystals. Phys Rev. 1947;71:809-1–16.
[42] Vinet P, Ferrante J, Rose JH, Smith JR. Compressibility of solids. J Geophys Res. 1987;92:9319–9326.
[43] Born M, Huang K. Dynamical theory of crystal lattices. New York, NY: Oxford University Press; 1988.
[44] Karki BB, Stixrude L, Clark SJ, et al. Structure and elasticity of MgO at high pressure. Am Mineral. 1997;82:51–60.
[45] Sin'ko GV, Smirnov NA. Ab initio calculations of elastic constants and thermodynamic properties of bcc, fcc and hcp Al crystals under pressure. J Phys Condens Matter. 2002;14:6989–7005.
[46] Feng LP, Liu ZT, Liu QJ. Structural, elastic and mechanical properties of orthorhombic SrHfO3 under pressure from first-principles calculations. Physica B. 2012;407:2009–2013.
[47] Haddadi K, Bouhemadou A, Louail L. Ab initio investigation of the structural, elastic and electronic properties of the anti-perovskite TlNCa3. Solid State Commun. 2010;150:932–937.
[48] Pugh SF. Relations between the elastic moduli and plastic properties of polycrystalline pure metals. Philos Mag. 1954;45:823–843.
[49] Anderson OL. A simplified method for calculating the Debye temperature from elastic constants. J Phys Chem Solids. 1963;24:909–917.
[50] Schreiber E, Anderson OL, Soga N. Elastic constants and their measurements. New York, NY: McGraw-Hill Companies; 1974.
[51] Ravindran P, Fast L, Korzhavyi PA, Johansson B, Eriksson O. Density functional theory for calculation of elastic properties of orthorhombic crystals: application to TiSi2. J Appl Phys. 1998;84:4891-1–14.
[52] Lloveras P, Castán T, Porta M, Planes A, Saxena A. Influence of elastic anisotropy on nanoscale textures, Phys. Rev. Lett. 2008;100:165707-1–4.
[53] Nye JF. Properties of crystals. New York, NY: Oxford University Press; 1985.